Analytical and Bioanalytical Chemistry
https://doi.org/10.1007/s00216-022-04368-x

RESEARCH PAPER

# Icosahedral gold nanoparticles decorated with hexon protein: a surrogate for adenovirus serotype 5

**Beatriz Fresco-Cala[1,2] · Ángela I. López-Lorente[2] · Alex D. Batista[1] · Mehmet Dinc[5] · Joachim Bansmann[3] · R. Jürgen Behm[3,4] · Soledad Cárdenas[2] · Boris Mizaikoff[1,5]**

Received: 20 June 2022 / Revised: 26 September 2022 / Accepted: 30 September 2022


## Abstract

The development of synthetic particles that emulate real viruses in size, shape, and chemical composition is vital to the development of imprinted polymer-based sorbent materials (molecularly imprinted polymers, MIPs). In this study, we address surrogates for adenovirus type 5 (Adv 5) via the synthesis and subsequent modification of icosahedral gold nanoparticles (iAuNPs) decorated with the most abundant protein of the Adv 5 (i.e., hexon protein) at the surface. CTAB-capped iAuNPs with dimensions in the range of 40–90 nm were synthesized, and then CTAB was replaced by a variety of polyethylene glycols (PEGs) in order to introduce suitable functionalities serving as anchoring points for the attachment of the hexon protein. The latter was achieved by non-covalent linking of the protein to the iAuNP surface using a PEG without reactive termination (i.e., methoxy PEG thiol, mPEG-SH, Mn=800). Alternatively, covalent anchoring points were generated by modifying the iAuNPs with a bifunctional PEG (i.e., thiol PEG amine, SH-PEG-$NH_2$) followed by the addition of glutaraldehyde. X-ray photoelectron spectroscopy (XPS) confirmed the formation of the anchoring points at the iAuNP surface. Next, the amino groups present in the amino acids of the hexon protein interacted with the glutaraldehyde. iAuNPs before and after PEGylation were characterized using dynamic light scattering (DLS), XPS, transmission electron microscopy (TEM), scanning electron microscopy (SEM), and UV–Vis spectroscopy, confirming the CTAB–PEG exchange. Finally, the distinct red shift obtained in the UV–Vis spectra of the pegylated iAuNPs in the presence of the hexon protein, the increase in the hydrodynamic diameter, the change in the zeta potential, and the selective binding of the hexon-modified iAuNPs towards a hexon-imprinted polymer (HIP) confirmed success in both the covalent and non-covalent attachment at the iAuNP surface.

**Keywords** Icosahedral gold nanoparticles · Hexon protein · Adenovirus serotype 5 · PEGylation · Hexon-imprinted polymer · Surrogate

In honor of Prof. Miguel Valcárcel.

Published in the topical collection *Analytical Nanoscience and Nanotechnology* with guest editors Ángel Ríos and Wolfgang J. Parak.

✉ Beatriz Fresco-Cala
q72frcab@uco.es

✉ Alex D. Batista
alex.domingues-batista@uni-ulm.de

[1] Institute of Analytical and Bioanalytical Chemistry, Ulm University, 89081 Ulm, Germany

[2] Departamento de Química Analítica, Instituto Universitario de Investigación en Química Fina y Nanoquímica IUNAN, Universidad de Córdoba, Campus de Rabanales, Edificio Marie Curie, E-14071 Córdoba, España

[3] Institute for Surface Chemistry and Catalysis, Ulm University, 89081 Ulm, Germany

[4] Institute of Theoretical Chemistry and Catalysis, Ulm University, 89069 Ulm, Germany

[5] Hahn-Schickard, 89077 Ulm, Germany

Published online: 24 October 2022

## Introduction

Epidemics and pandemics have always been a part of humanity, changing the history and development of civilizations [1]. While we currently suffer from the COVID-19 pandemic, many other viruses such as influenza, smallpox, human immunodeficiency virus (HIV), or adenoviruses (Adv) have affected many people for decades and have become a serious health threat to the population. In particular, Advs are largely resistant to external agents, since they do not have a lipid envelope. This makes them easily transmissible both by inhalation and by the fecal–oral route [2, 3]. Therefore, this type of virus mainly causes infections of the upper respiratory and digestive tracts [4]. Advs are non-enveloped viruses, which consist of an icosahedral capsid with a 34 to 36 kb linear double-stranded DNA genome inside [5]. Their capsid is formed by three major proteins including hexon, penton base, and fiber [6]. Among them, the hexon protein is the main component of the capsid, and therefore plays a pivotal role in the development of the immune response [7–9].

The development of safe and scalable synthetic viruses (a.k.a., virus surrogates) will allow their use in laboratories with minimal biosafety requirements, and may therefore serve a wide range of biomedical and material applications [10–13]. The infectious nature of viruses, as well as their fragility and low stability in organic solvents and at non-biological conditions, renders synthetic substitutes, which have the same size, shape, and surface functionality, a research field of major interest [14, 15]. In particular, they can be especially useful in the development of imprinted polymer-based sorbent materials (molecularly imprinted polymers, MIPs) with virus recognition properties. This innovative strategy would consist of replacing the template (real virus), which is needed to create the specific binding sites in the polymer, with these robust and non-infectious synthetic virus surrogates during the polymerization step. Given the similarity on the dimensional scale, nanotechnological approaches are the most promising route towards synthetic virus surrogates. Gold nanoparticles (AuNPs) are among the most widely used nanomaterials in biomedical applications, including drug and gene delivery [16, 17], imaging/diagnostics [18–20], and photodynamic/photothermal therapies [21, 22]. This ubiquitous utility results from specific features of AuNPs including their outstanding optical and photothermal properties, their high affinity for binding of/to a wide variety of (bio) molecules given their flexible surface chemistry, and the facile control of the synthesis conditions to obtain a wide variety of particles shapes and sizes [23, 24]. The interaction between biological systems and AuNPs mainly depends on the type of (bio)molecule adsorbed onto the nanoparticle surface. In the case of attached proteins, they not only provide stabilization and dispersibility of AuNPs, but frequently also improve their biocompatibility [25, 26]. Proteins can bind to the AuNP surface via covalent bonds or physical interactions [27], which largely determines the density of the protein coating as well as the reversibility of the surface decoration. The type of binding mainly depends on the structure and/or reactivity of the surfactant used to prepare/stabilize the AuNPs [28–30]. Among the most common surfactants, cetyltrimethylammonium bromide (CTAB) stands out as it is widely used, especially in the synthesis of non-spherical AuNPs, such as nanorods and icosahedral AuNPs [31–34]. However, its high cytotoxicity and possible interference with established protein linking protocols has led to its replacement by more biocompatible surface ligands, such as thiol-terminated polyethylene glycol (e.g., mPEG-SH or SH-PEG-$NH_2$) [35, 36].

The present study evaluates the effectiveness of decorating the surface of icosahedral AuNPs (iAuNPs) by the hexon protein characteristics of adenovirus serotype 5 (Adv 5), to obtain virus surrogate particles, which emulate the shape, size, and chemical surface composition of Adv 5. For this purpose, a novel protocol for the PEGylation of icosahedral, initially CTAB-capped iAuNPs has been developed, obtaining stable pegylated so-called iAuNPs. The CTAB-capped iAuNPs were modified using different types of thiol-terminated polyethylene glycols including methoxy-PEG-thiol (mPEG-SH) and thiol-PEG-amine (SH-PEG-$NH_2$), as well as 50:50 mixtures of these PEGs. When mPEG-SH was used, hexon protein interacted with the iAuNPs via non-covalent and, therefore, reversible forces. In contrast, when iAuNPs were functionalized with SH-PEG-$NH_2$ and subsequently interacted with glutaraldehyde, hexon protein linked covalently to them. All pegylated iAuNPs were characterized using transmission electron microscopy (TEM), scanning electron microscopy (SEM), dynamic light scattering (DLS), UV–Vis spectroscopy, and X-ray photoelectron spectroscopy (XPS) to confirm the replacement of CTAB by PEGs. UV–V is spectroscopy and DLS were also applied to confirm the interaction between the pegylated iAuNPs and the hexon protein. Finally, a binding study with hexon-imprinted polymers (HIPs) and their corresponding non-imprinted polymers (NIPs) was carried out using the prepared pegylated and hexon-modified iAuNPs as surrogate analytes (instead of the real Adv5).

## Materials and methods

### Reagents and materials

Reagents required for the preparation of the iAuNPs, including trisodium citrate, sodium borohydride, ascorbic acid, and CTAB, were purchased from Sigma-Aldrich. Hydrogen tetrachloroaurate (III) hydrate was obtained from Acros Organics. Poly(ethylene glycols) employed for the PEGylation (HS-PEG-$NH_2$ with average Mn 2000 and mPEG-SH with average Mn 800) and glutaraldehyde were purchased from Sigma-Aldrich. Purified hexon protein from adenovirus

type 5 (Adv5) (purified adenovirus type 5 hexon-liquid prepared in 10 mM bis-tris propane buffer, 375 mM NaCl at a concentration of 0.39 mg $mL^{-1}$) was supplied by Bio-Rad. Protein LoBind tubes of 1.5, 2, and 15 mL from VWR were used for all experiments.

## Instrumentation

A Vortex-Genie 2 mixer was used to shake the NP dispersions during the PEGylation procedure. A JOEL JEM-1400 TEM was used to obtain information about the size and shape of the synthesized iAuNPs. Therefore, a drop of the NP dispersion was placed on a copper grid and then dried to retain the particles on the grid. A Helios NanoLab 600 SEM was also employed for the characterization of the pegylated iAuNPs and to observe the interaction of hexon-modified iAuNPs with hexon-imprinted polymers and their corresponding non-imprinted polymers.

To confirm the exchange of CTAB by the PEGs after the PEGylation protocol, DLS and zeta potential measurements of iAuNP dispersions were performed with a Zetasizer Nano ZSP (Malvern Panalytical, Herrenberg, Germany). Measurement parameters were as follows: a laser wavelength of 632 nm (He-Ne), scattering angle of 173°, measurement temperature of 25 °C, viscosity of 0.8872 mPa·s, dispersant refractive index of 1.33, and material refractive index of 0.2. A disposable polystyrene cuvette (minimum volume 1 mL) was used for the measurements. UV-Vis spectroscopy (SPECORD S6000, Analytik Jena, Germany) was also used for the characterization of pegylated iAuNPs. The measurements were performed with 0.7 mL of the solution in a Suprasil quartz glass cuvette, with a volume of 0.7 mL and an optical path length of 2 mm (Hellma Analytics, Müllheim, Germany).

XPS was used to confirm the formation of the imine bond between SH-PEG-$NH_2$-coated iAuNPs and glutaraldehyde. The measurements were performed on a PHI 5800 ESCA system (Physical Electronics) using monochromatic Al-Kα radiation (1486 eV). Survey spectra were recorded with a pass energy of 93.9 eV and detail spectra with 29.35 eV. The binding energies (BEs) of all spectra were calibrated against the C 1*s* peak of adventitious carbon, which was fixed at a binding energy of 284.8 eV.

## Preparation of pegylated-icosahedral gold nanoparticles

Icosahedral CTAB-capped iAuNPs were synthesized following a method previously reported in the literature [30]. Thereafter, CTAB that covered the iAuNPs after the synthesis was exchanged for PEGs. For this exchange reaction, a novel protocol based on a slow exchange of these surfactants (i.e., this process was carried out for 3 days) was developed and optimized to ensure the stability of iAuNPs when removing CTAB from their surface. As schematically shown in Fig. S5, the steps of this PEGylation process were as follows: (i) 1 mL of an aqueous dispersion of CTAB-iAuNPs at a concentration of 17.4 nM was centrifuged at 5500 rpm for 20 min. The supernatant was removed, and the CTAB-iAuNPs were redispersed in 1 mL of water. (ii) Next, 25 µL of PEGs (mPEG-SH, SH-PEG-$NH_2$ or the 50:50 mixture of both), which were prepared at a concentration of 2 mM in water, were sequentially added to the dispersion every 24 h for 3 days while the dispersion was incubated with shaking. (iii) After the last addition of PEGs, the dispersion was incubated for 6 h, centrifuged, and the supernatant removed in order to eliminate any excess of CTAB. The partially pegylated iAuNPs were dispersed in 450 µL of water and 25 µL of 2 mM PEGs, and were incubated overnight. Thereafter, the dispersion of the pegylated iAuNPs was again centrifuged and the final supernatant removed. The pegylated iAuNPs were finally dispersed in water or PBS depending on whether they were characterized or used for the following experiments. This procedure was carried out with iAuNPs with sizes of 40 and 90 nm, respectively.

## Non-covalent attachment of hexon protein from Adv 5 to pegylated iAuNPs

Hexon protein was linked to the mPEG-SH-coated iAuNPs by non-covalent interactions. iAuNPs coated with mPEG-SH were dispersed in 1 mL of PBS, and then 40 µL of hexon protein solution was directly added to this dispersion. This mixture was incubated for 1 h with shaking using a vortex at 500 rpm. Afterwards, the dispersion was centrifuged for 20 min at 5500 rpm. The supernatant was removed, and the nanoparticles were redispersed in 1 mL of PBS.

## Covalent attachment of hexon protein from Adv 5 to pegylated iAuNPs

To anchor the hexon protein covalently to iAuNPs, they were coated with a bifunctional PEG (i.e., SH-PEG-$NH_2$). For this purpose, both the iAuNPs coated only with SH-PEG-$NH_2$ and iAuNPs coated with a 50:50 mixture of mPEG-SH:SH-PEG-$NH_2$ were dispersed in 1 mL of PBS. Next, 10 µL of glutaraldehyde was added to the dispersion and shaken at 500 rpm for 2 h, after which this mixture was centrifuged for 20 min at 5500 rpm, and the nanoparticles were dispersed in 1 mL of PBS. Then, 40 µL of hexon protein solution was added to the PBS dispersion of the pegylated iAuNPs modified with glutaraldehyde and incubated for 1 h at 500 rpm. Finally, the mixture was again centrifuged, removing the

supernatant containing any excess unreacted hexon protein, and was redispersed in 1 mL of PBS.

## Results and discussion

### Synthesis, PEGylation, and characterization of iAuNPs

The main objective of this study was the preparation of synthetic surrogate adenovirus particles using iAuNPs. AuNPs are excellent candidates for this purpose due to their biocompatibility, the ease of anchoring proteins at their surface, and the versatility of their synthesis. The latter allows a wide variety of dimensions and geometries to be obtained. In the present case, AuNPs with an icosahedral shape were selected because they perfectly emulate the shape and size of Adv 5. iAuNPs were successfully prepared with controlled dimensions from 40 to 90 nm, adapting an aqueous phase seed-mediated growth approach [33]. First, AuNP seeds were prepared by reduction of $HAuCl_4$ with sodium borohydride. Next, these seeds were mixed with a growth solution consisting of CTAB (capping agent), $HAuCl_4$ (gold source), and ascorbic acid (reducing agent), yielding icosahedral AuNPs with larger dimensions. The size of these iAuNPs can be tailored by controlling the density of seeds and the amount of growth solution used. TEM micrographs of the iAuNPs with sizes from 40 to 90 nm are illustrated in Fig. S1. In addition, UV–Vis spectra of iAuNPs were recorded (Fig. S1), confirming different transverse surface plasmon resonances (SPR $\lambda_{max}$) according to the size. These iAuNPs were coated with a CTAB bilayer (i.e., capping agent used during the synthesis), and therefore revealed positive zeta potentials (33.93 ± 4 mV and 47.5 ± 2 mV for iAuNPs with average diameters of 40 nm and 90 nm measured by TEM, respectively). As expected, DLS measurements gave on average higher diameter values (i.e., 44 ± 1 nm and 97 ± 1 nm) than the dimensions derived from the TEM images, since the hydrodynamic diameter also comprises the layer of CTAB that surrounds the iAuNPs. Taking into account that the size of Adv 5 ranges between 60 and 90 nm, only the smallest iAuNPs (i.e., TEM diameter of 40 nm and hydrodynamic diameter derived from DLS of 44 nm) were used for further experiments (i.e., immobilization of hexon protein at their surface). The monodisperse size is one of the most important features of viruses. Figure 1 shows TEM and SEM images of the prepared iAuNPs which demonstrate that they have a homogeneous size and shape.

In addition to emulating Adv 5 in shape and size, one of the main objectives of this study was to anchor the most prevalent protein at the surface of Adv 5 (i.e., hexon protein) capping at the surface of iAuNPs in order to finally obtain iAuNPs that were similar in terms of surface chemistry. However, once hexon protein was added to the iAuNP dispersion, no interaction was observed. Figure S2 shows images of the dispersion of CTAB-capped iAuNPs incubated with different volumes of hexon protein (i.e., from 1 to 10 µL hexon protein per 250 µL of iAuNP dispersion). As evident, no color change was observed. Furthermore, UV–Vis spectra of these dispersions (Fig. S3) revealed that the transverse SPR $\lambda_{max}$ (at approx. 526 nm) was practically the same for all dispersions (i.e., including the dispersion of iAuNPs without protein, referred to as "CTAB reference"). These findings indicated that there was no significant interaction between the nanoparticles and protein.

Hence, a new strategy for the attachment (i.e., both covalent and non-covalent, respectively) of hexon protein at the iAuNPs surface was developed. This strategy hinges on the replacement of the CTAB of the iAuNP surface by PEGs (SH-PEG-$NH_2$ and mPEG-SH) via a novel protocol, as previously described and shown in detail in Fig. S4. Although some authors have proposed faster PEGylation protocols for spherical and rod-shaped AuNPs, which are based on the addition of small amounts of ethanol [37], the presence of other surfactants [35] or via a change in the pH of the medium for the PEGylation [29], none of these approaches worked for icosahedral AuNPs as synthesized herein. It is hypothesized that their relatively large dimensions along with the geometry (i.e., number of tips and edges) may cause instability and/or irreversible aggregation effects if CTAB

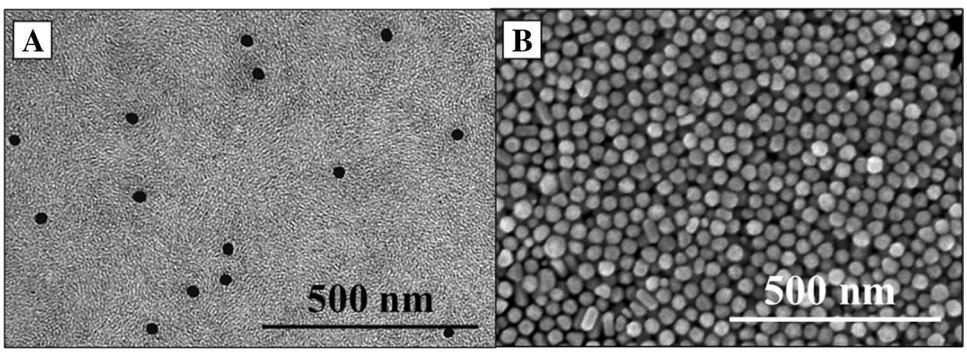


**Fig. 1** (**A**) TEM and (**B**) SEM micrographs of the synthesized iAuNPs with size of 40 nm

is rapidly removed from the surface (Fig. S5). Although the PEGylation results shown throughout this work are those obtained for iAuNPs with an average size of 40 nm, the developed 3-day PEGylation protocol was also successfully applied to iAuNPs with larger dimensions (90 nm), which also remained stable during and after CTAB-PEG exchange (Fig. S6).

On the one hand, iAuNPs coated with a monofunctional PEG with an average molecular mass of 800 (mPEG-SH) were prepared. mPEG-SH was linked to the gold surface via the thiol group. Therefore, hexon protein can interact with the hydrocarbon chain via non-covalent interactions [38]. The resulting mPEG-SH-coated iAuNPs were stable without limitations, and no aggregation was observed after the PEGylation (Fig. S6). After analysis by DLS, the zeta potentials and dimensions summarized in Table 1 were obtained. As expected, the zeta potential decreased with the introduction of mPEG-SH on the surface of the iAuNPs, showing a nearly neutral surface [36, 39]. As evident in the UV–Vis spectra (Fig. S7), slight blue shifts in the transverse SPR were obtained after the PEGylation. This behavior has also been reported previously after the replacement of CTAB by PEGs, and it is consistent with the smaller size of the mPEG-SH-capped iAuNPs [35, 39]. Figure S7 also clearly indicates the disappearance of the CTAB-associated peak (at approx. 200 nm) after PEGylation.

On the other hand, to create covalent anchoring points for the hexon protein at the iAuNP surface, a longer-chain bifunctional PEG (SH-PEG-$NH_2$ with an average molecular mass of 2000) was used for providing an initial surface architecture. SH-PEG-$NH_2$ was anchored to the metal surface via the thiol group, leaving a reactive amine group at the distal end replacing the CTAB present at the iAuNP surface. Next, glutaraldehyde was linked to the iAuNPs by reaction with the free amine group of SH-PEG-$NH_2$, thus allowing the covalent attachment of the hexon protein [40–42]. After the PEGylation protocol, the resulting iAuNPs coated with SH-PEG-$NH_2$ were stable for months, and no aggregates were observed in the stored dispersions (Fig. S6). To confirm the exchange of CTAB by the bifunctional PEG, SH-PEG-$NH_2$-coated iAuNPs were characterized by DLS and UV–Vis spectroscopy. As shown in Table 1, the zeta potential decreased from 33.93 mV (for CTAB-iAuNPs) to 26.76 mV (for SH-PEG-$NH_2$-coated iAuNPs). These values fit with the theoretically expected values, since SH-PEG-$NH_2$ is positively charged just as CTAB [29]. The average hydrodynamic diameter of SH-PEG-$NH_2$-coated iAuNPs (50 nm) obtained in the DLS measurement was slightly higher than that of the mPEG-SH-coated iAuNPs (41 nm) (Table 1). A small blue shift was also obtained in the UV–Vis spectrum of the SH-PEG-$NH_2$-coated iAuNPs in comparison with the CTAB-iAuNPs (Fig. S7). It should be noted that the CTAB-associated absorption peak (at approx. 200 nm) disappeared after the PEGylation procedure.

In addition, pegylated iAuNPs were prepared using a 50:50 mixture of SH-PEG-$NH_2$ and mPEG-SH following the same 3-day protocol. Stable pegylated iAuNPs were again obtained. The zeta potential and the average hydrodynamic diameters derived from DLS measurements for iAuNPs coated with 50:50 of SH-PEG-$NH_2$ and mPEG-SH are listed in Table 1. An intermediate value of the zeta potential was obtained when both PEGs were used. Also, the hydrodynamic diameter of iAuNPs functionalized with both PEGs consistently lay between the values derived for iAuNPs modified only with mPEG-SH or SH-PEG-$NH_2$. The UV-Vis spectrum of 50:50 functionalized iAuNPs is also shown in Fig. S7. SEM micrographs of pegylated iAuNPs are shown in Fig. S8.

The stability of all pegylated iAuNPs and CTAB-iAuNPs was tested in the presence of a high concentration of salt (100 g/L of NaCl). The results confirmed the successful exchange of CTAB by PEGs, since all PEG-coated iAuNPs were stable after the addition of the salt, maintaining the same pink color for more than a month. On the contrary, the pink color of the dispersion of CTAB-iAuNPs disappeared after a few minutes of incubation in the presence of NaCl. These results confirm that the PEGylation not only introduced anchoring points for hexon protein at the surface of iAuNPs, but also led to an increase in stability under physiological salt conditions [43].

**Table 1** Average diameters (in terms of intensity) calculated from the DLS measurements and zeta potential of pegylated iAuNPs with and without hexon protein ($n$=3 for each experiment; results indicate the average value ± standard deviation of the different measurements)

| Sample | Before incubation with hexon protein | | After incubation with hexon protein | |
|---|---|---|---|---|
| | Average diameter (nm) | Zeta potential (mV) | Average diameter (nm) | Zeta potential (mV) |
| iAuNPs[a] with 100% of mPEG-SH | 41 ± 1 | 10 ± 1 | 55 ± 1 | −20.5 ± 0.5 |
| iAuNPs[a] with 100% of SH-PEG-$NH_2$ | 50 ± 1 | 35 ± 5 | - | - |
| iAuNPs[a] with 50% of SH-PEG-$NH_2$ and 50% of mPEG-SH | 48 ± 2 | 14 ± 2 | 57 ± 2 | −14 ± 1 |

## Non-covalent attachment of hexon protein to pegylated iAuNPs

Non-covalent attachment of hexon protein was achieved by adding hexon solution to 0.25 mL of PBS dispersion of mPEG-SH-coated iAuNPs. The effect of the amount of the added hexon protein was evaluated in the range of 0–10 µL (Table S1). A small shift of the SPR $\lambda_{max}$ towards red was obtained with the addition of up to 5 µL of hexon solution. However, as is evident in Fig. 2, once 10 µL of hexon solution was added, the SPR $\lambda_{max}$ was 536 nm and the red shift obtained reached 11 nm. Along with the red shift in the UV–Vis spectrum, a small color change was observed in the dispersion, which also revealed the interaction between hexon protein and the mPEG-SH-coated iAuNPs. However, the red shift of the plasmon peak and the color change could also be due to aggregation/agglomeration of the iAuNPs. To distinguish between these scenarios, DLS measurements were also carried out, and both the increase in the hydrodynamic size and the decrease in the zeta potential (the zeta potential of an aqueous solution of hexon protein is −13.6 mV) confirmed the presence of the protein at the surface of pegylated iAuNPs. DLS graphs of the iAuNPs before and after the non-covalent attachment of the protein are shown in Fig. S9. Hexon protein-PEG-iAuNPs complexes were also characterized by TEM; however, no significant differences before and after protein attachment were observed (Figs. 1, S1 and S10). Since mPEG-SH does not have a functional group at its distal end, the interaction with the protein is non-covalent, i.e., mainly via hydrophobic interactions [38]. It should also be noted that the stability of the dispersion was not affected by the formation of the protein–nanoparticle complex.

## Covalent attachment of hexon protein to pegylated iAuNPs

After the modification of iAuNPs with 100 wt% of SH-PEG-$NH_2$, covalent anchoring points for the hexon protein were generated at the nanoparticle surface after the addition of glutaraldehyde to an aqueous dispersion of SH-PEG-$NH_2$-coated iAuNPs. Glutaraldehyde interacts with amino groups present in the amino acids of the protein [44, 45]. XPS analysis of the SH-PEG-$NH_2$ pegylated iAuNPs before and after the addition of glutaraldehyde was performed. C 1*s* spectra before and after the addition of the glutaraldehyde showed differences (Fig. S11). The C 1*s* spectrum of pegylated iAuNPs before the addition of glutaraldehyde showed peaks related to C–C/C–H groups (285.0 eV) and C–O/C–N groups (286 eV). A shoulder at 283 eV we attribute to an artifact related to the supporting Si wafer. After adding the glutaraldehyde, a new C 1*s* peak at 287 eV was observed. This peak can be assigned to the C=O groups in glutaraldehyde or C=N groups arising from an imine bond between SH-PEG-$NH_2$ and the glutaraldehyde. Additionally, Fig. S12 illustrates the XPS results for the chemical states of nitrogen with and without glutaraldehyde. The N

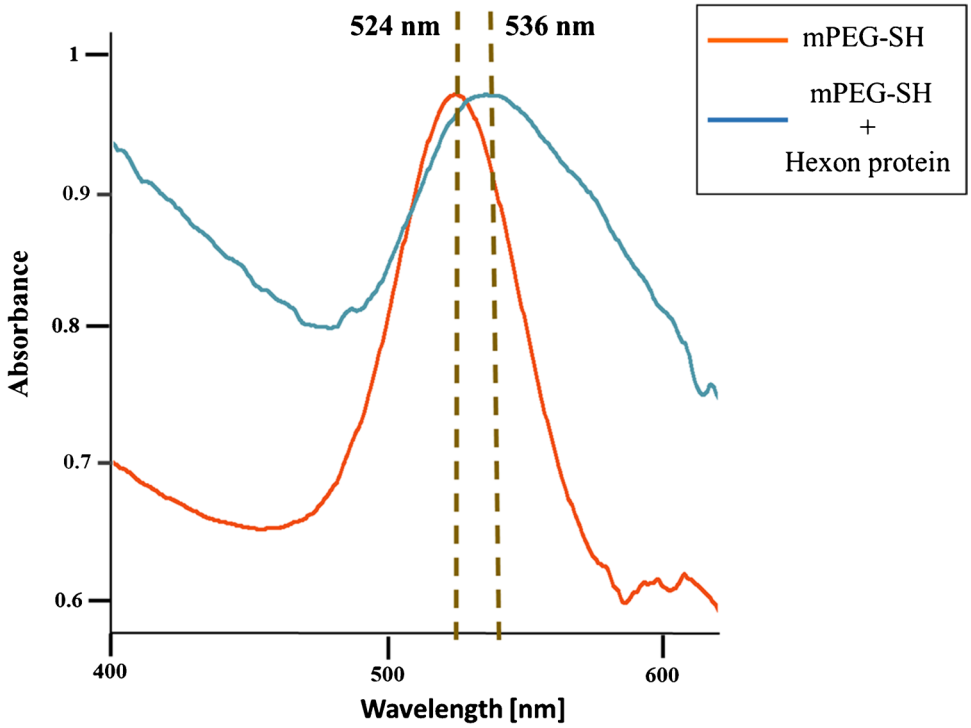


**Fig. 2** Normalized UV–Vis spectra of mPEG-SH-coated iAuNPs before and after incubation with hexon protein

1*s* spectrum of pegylated iAuNPs showed only a peak at 401.8 eV, which is assigned to the amine groups of the SH-PEG-$NH_2$. Indeed, a new peak at 399.5 eV (from the imine group, C=N–C) was obtained in the N 1*s* spectrum of the pegylated iAuNPs modified with glutaraldehyde, providing clear evidence for the formation of an imine bond between SH-PEG-$NH_2$ and glutaraldehyde. These changes at the core–level regions of the C 1*s* and N 1*s* demonstrated the successful formation of the imine group, and therefore the creation of covalent anchoring points at the nanoparticle surface for further attachment of the hexon protein.

In order to achieve high yields of hexon protein immobilization at the iAuNPs, the amount of both glutaraldehyde and the hexon protein were optimized. Thus, the addition of different volumes of glutaraldehyde in the range of 2–10 µL per mL of iAuNP dispersion was tested (Table S1). In addition, the influence of adding different volumes of hexon protein solution was evaluated in the interval of 1–10 µL per 0.25 mL of iAuNP dispersion (Table S1). In all cases, regardless of the amount of glutaraldehyde and the amount of hexon protein, the added nanoparticles stuck to the walls of the tubes, leaving a transparent solution (Fig. S13). Although the SH-PEG-$NH_2$-pegylated iAuNPs apparently interacted with hexon protein, destabilization was observed. Unfortunately, SH-PEG-$NH_2$-iAuNPs with attached hexon protein could not be separated and recovered from the inner wall of the tubes. In contrast, this did not occur with the iAuNPs functionalized with the 50:50 mixture of both PEGs (50/50-pegylated iAuNPs). In this case, the effect of the addition of different amounts of glutaraldehyde and hexon protein was also studied. The $\lambda_{max}$ values obtained for the transverse SPRs are listed in Table S1. If the amount of glutaraldehyde was increased from 2 to 10 µL, a slight red shift was observed when adding hexon protein. However, this change was not sufficient to indicate an interaction of 50/50-pegylated iAuNPs with the protein. No color changes were observed in these iAuNP dispersions after incubation with hexon protein. On the other hand, keeping the amount of glutaraldehyde constant using a variety of concentrations of hexon protein was also tested. In all cases, the SPR $\lambda_{max}$ remained unchanged except upon addition of 10 µL of glutaraldehyde and an exceptionally high volume of hexon protein (10 µL). In this case, a significant red shift was observed. As can be seen in the Fig. 3, the transverse SPR $\lambda_{max}$ increased by approximately 12 nm (i.e., to 537 nm), and visually a distinct color change was observed. This fact could indicate that hexon protein indeed interacted with the pegylated iAuNPs modified with a 50:50 mixture of PEGs. The role of the mPEG-SH is not totally clear, but its presence prevents the destabilization of the dispersion after the attachment of the hexon protein. Presumably, it is placed at the surface of the iAuNPs between the SH-PEG-$NH_2$ chains, acting as a spacer without interacting with the hexon protein (note that the size of mPEG-SH, Mn=800, is about half the size of SH-PEG-$NH_2$, Mn=2000).

To confirm that this shift in UV–Vis was actually caused by the presence of the protein on the surface of the iAuNPs and not by aggregation problems, DLS measurements were also performed. Thus, the presence of the hexon protein was also demonstrated thanks to the DLS results, which showed the expected increase in the hydrodynamic diameter as well as the change to a negative zeta potential (since the zeta

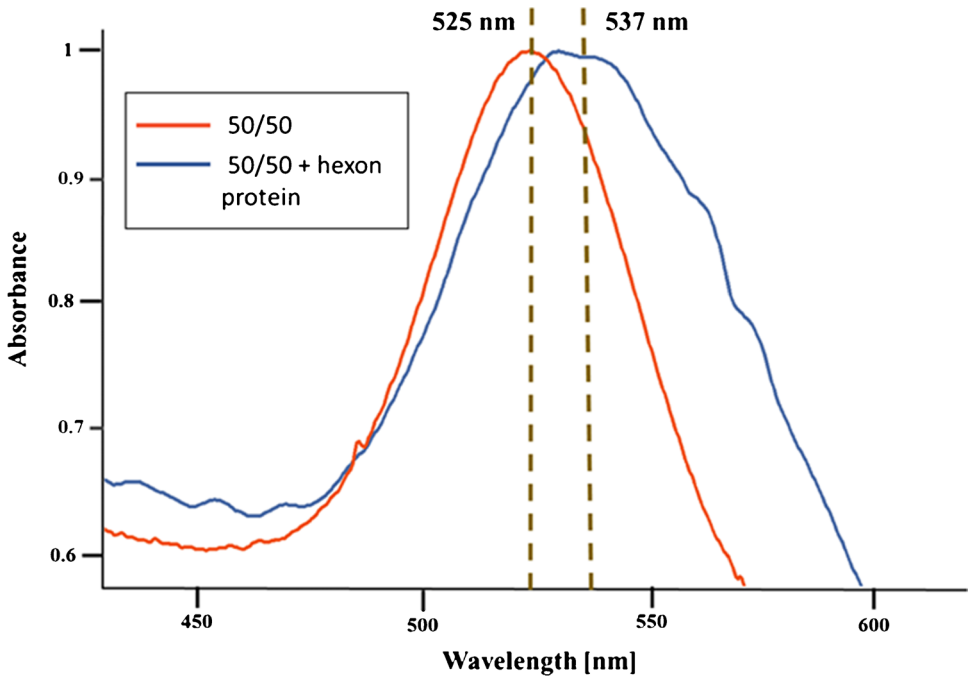


**Fig. 3** Normalized UV–Vis spectra of SH-PEG-$NH_2$-coated iAuNPs before and after incubation with hexon protein

potential of the hexon protein is −13.6 mV). Figure S14 shows the DLS graphs for iAuNPs with 100 wt% of SH-PEG-$NH_2$ and 50/50-pegylated iAuNPs before and after the attachment of the hexon protein. TEM micrographs of the iAuNPs after the covalent attachment of the protein are shown in Fig. S10.

### Hexon-modified iAuNPs as Adv 5 surrogates

The potential of the synthesized iAuNPs (before and after protein attachment) to act as surrogates for Adv 5 was evaluated by studying their interaction with a hexon protein-selective polymer. For that, a HIP and its corresponding NIP were prepared following a route previously published by our group [46]. Pegylated iAuNPs (100 wt% of mPEG-SH and 50/50 w/w% of mPEG-SH/SH-PEG-$NH_2$) with and without hexon protein at their surface were mixed with the HIP/NIP, respectively. These mixtures were incubated for 2 h at room temperature with shaking using a vortex at 500 rpm, and subsequently were characterized by SEM. Figure 4 shows that the iAuNPs decorated with hexon were linked to the HIP surface, while this did not happen for the pegylated iAuNPs (mPEG-SH- and 50/50-pegylated iAuNPs). Moreover, SEM micrographs of the interaction of both hexon-modified iAuNPs and non-modified iAuNPs with the NIP can be found in Fig. S15. In general, the SEM micrographs (Figs. 4 and S15) revealed that none of the pegylated iAuNPs bound to the HIP/NIP, since they were found on the support rather than attached to the silica spheres. However, hexon-modified iAuNPs showed high affinity for the HIP but not for the NIP, mimicking the real behavior expected for the Adv 5.

These results confirmed that only the iAuNPs with hexon protein showed a high affinity towards the HIPs, emulating the expected behavior of the real Adv 5.

iAuNPs decorated with hexon protein emulating adenoviruses represent only a starting point for the generic development of synthetic surrogate virus particles. AuNPs can be synthesized in a variety of ways, allowing them to emulate a wide range of virus dimensions and shapes. For example, rod-shaped AuNPs could act as surrogates for the tobacco mosaic virus, while spherical AuNPs with the correct diameter and decorated with SPIKE protein could mimic SARS-CoV-2. The opportunity of using synthetic non-infectious substitutes for SARS-CoV-2 that behave similarly in a biological medium will allow a significantly larger number of laboratories without requirement for strict biosafety measures to handle surrogate materials, which will accelerate the development of new detection methods or vaccines, as well as gaining mechanistic insight into the interaction of a virus surrogate with other biological components.

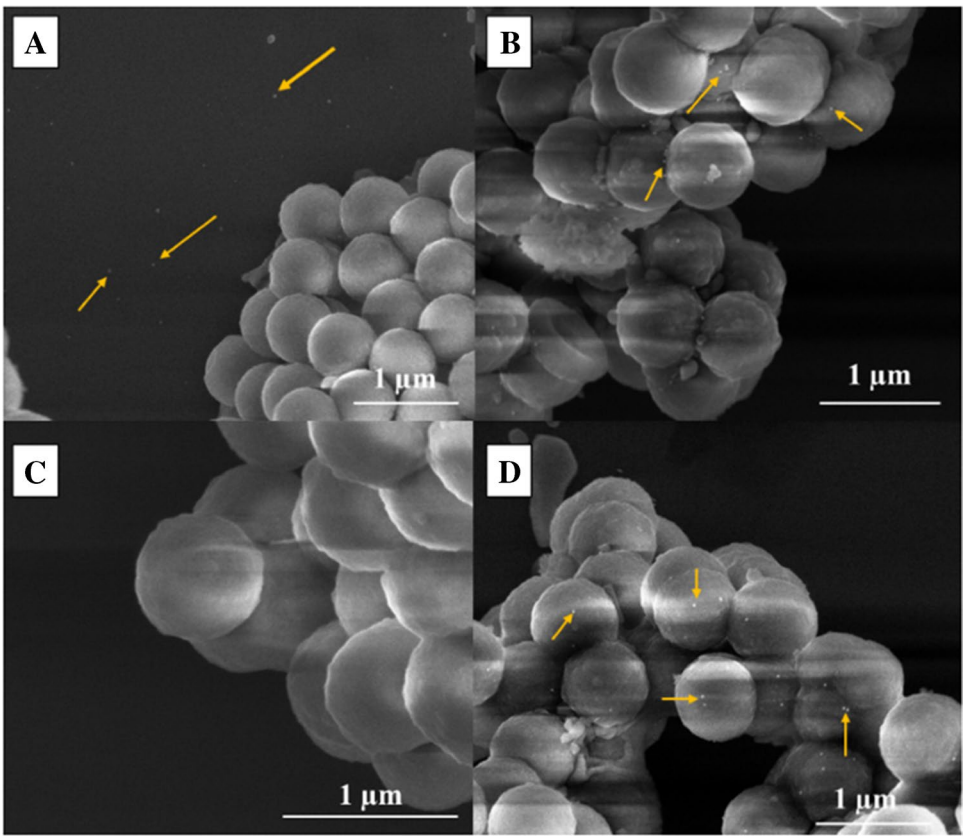


**Fig. 4** SEM micrographs of the HIP after incubation with (**A**) the mPEG-SH-pegylated iAuNPs, (**B**) the mPEG-SH-pegylated iAuNPs modified with hexon protein, (**C**) the mPEG-SH/SH-PEG-$NH_2$-pegylated iAuNPs, and (**D**) the mPEG-SH/SH-PEG-$NH_2$-pegylated iAuNPs modified with hexon protein. Yellow arrows highlight the position of the iAuNPs

## Conclusions

The successful production of virus-imprinted polymers requires an appropriate imprinting approach, as the use of entire viruses as template species is a critical step owing to their vulnerability under polymerization conditions. Additionally, the direct use of harmful (i.e., infectious) viruses serving as templates during imprinting may carry a risk of infection during the synthesis. To date, only a small number of publications have reported the synthesis of materials selectively binding specific viruses, which may be attributed to the rather delicate or infectious template. Hence, an alternative imprinting method whereby the virus is replaced by a robust and non-infectious synthetic surrogate template emulating in size, shape, and surface functionality the actual virus appears highly intriguing.

Surrogates for Adv 5 using icosahedral AuNPs decorated with hexon protein—the most abundant protein at the Adv 5 surface—have been developed. iAuNPs in the same size range as Adv 5 were synthesized. Since these iAuNPs were capped with CTAB for stabilization, a replacement strategy with a variety of PEGs was developed. Then, hexon protein was interacted with the PEGs via either covalent or non-covalent interactions and immobilized at the iAuNP surface. Once the surface of the iAuNPs was decorated with the hexon protein, a surrogate particle with size, shape, and chemical surface functionality similar to Adv 5 was obtained.

The developed PEGylation protocol was successful in replacing CTAB at the surface of iAuNPs with dimensions ranging from 40 to 90 nm. This demonstrates the generic potential of the proposed new PEGylation strategy and represents a general breakthrough for the replacement or exchange of toxic capping agents such as CTAB by biocompatible stabilizers such as PEGs at AuNPs with large dimensions and non-spherical shapes. Additionally, the obtained results confirmed that, as a result of the PEGylation, not only were anchoring points for hexon protein introduced at the surface of iAuNPs, but an increase in stability under physiological salt conditions was also achieved.

The hexon-modified pegylated iAuNPs showed a high affinity towards HIPs, while they were not linked to the NIPs. In contrast, iAuNPs without hexon protein on their surface did not bind to HIPs/NIPs. This demonstrates that only the iAuNPs decorated with the hexon protein behave in the presence of HIP/NIP similar to what is expected for real Adv 5, allowing their use as surrogate synthetic viruses.

The proposed approach for the preparation of these surrogate particles can be extended to the development of AuNPs with alternative geometries and dimensions, which in turn can be decorated with a variety of proteins depending on the virus of interest. This strategy opens the door to emulation of a wide range of viruses including contemporary specimens such as SARS-CoV-2. Consequently, our research team is currently working on obtaining surrogate AuNPs for SARS-CoV-2 based on the encouraging fundamental results obtained during the present study. As a future perspective, it would be interesting to decorate the surface of AuNPs with more than one type of protein, i.e., immobilizing the two or three most relevant proteins representing the surface of a target virus to generate surrogate particles with even closer resemblance to virus-like properties.

**Supplementary Information** The online version contains supplementary material available at https://doi.org/10.1007/s00216-022-04368-x.

**Acknowledgments** B. Fresco-Cala and A.D. Batista thank the Alexander von Humboldt Foundation for the Humboldt Research Fellowship for Postdoctoral Researchers at the Institute of Analytical and Bioanalytical Chemistry, Ulm University, Germany. This work was in part supported by the Ministerium für Wissenschaft, Forschung und Kunst (MWK) Baden-Württemberg within the specific funding line 'Research on Covid-19'. Funding received from the financial Support Programmes for Female Researchers, Office for Gender Equality (Ulm University) is also gratefully acknowledged.

**Funding** Ministerium für Wissenschaft, Forschung und Kunst (MWK) Baden-Württemberg within the specific funding line 'Research on Covid-19'.

Financial Support Programmes for Female Researchers, Office for Gender Equality (Ulm University, Germany).

## Declarations

**Conflicts of interest** The authors declare that there are no conflicts of interest.

## References

1. Jones RA. Global plant virus disease pandemics and epidemics. Plants. 2021;10(2):233.
2. Crabtree K, Gerba C, Rose J, Haas C. Waterborne adenovirus: a risk assessment. Water Sci Technol. 1997;35(11-12):1–6.
3. Lichtenstein DL, Wold WS. Experimental infections of humans with wild-type adenoviruses and with replication-competent adenovirus vectors: replication, safety, and transmission. Cancer Gene Ther. 2004;11(12):819.
4. Ghebremedhin B. Human adenovirus: viral pathogen with increasing importance. Eur J Immunol. 2014;4(1):26–33.
5. Nemerow GR, Stewart PL, Reddy VS. Structure of human adenovirus. Curr Opin Virol. 2012;2(2):115–21.
6. Russell W. Adenoviruses: update on structure and function. J Gen Virol. 2009;90(1):1–20.
7. Pichla-Gollon SL, Drinker M, Zhou X, Xue F, Rux JJ, Gao G-P, et al. Structure-based identification of a major neutralizing site in an adenovirus hexon. J Virol. 2007;81(4):1680–9.
8. Liu H, Jin L, Koh SBS, Atanasov I, Schein S, Wu L, et al. Atomic structure of human adenovirus by cryo-EM reveals interactions among protein networks. Sci. 2010;329(5995):1038–43.
9. Kalyuzhniy O, Di Paolo N, Silvestry M, Hofherr S, Barry MA, Stewart P, et al. Adenovirus serotype 5 hexon is critical for virus infection of hepatocytes in vivo. Proc Natl Acad Sci. 2008;105(14):5483–8.

10. Mohsen MO, Speiser DE, Knuth A, Bachmann MF. Virus-like particles for vaccination against cancer. Wiley Interdisciplinary Rev: Nanomed Nanobiotechnol. 2020;12(1):e1579.
11. Qian C, Liu X, Xu Q, Wang Z, Chen J, Li T, et al. Recent progress on the versatility of virus-like particles. Vaccines. 2020;8(1):139.
12. Mastrobattista E, van der Aa MA, Hennink WE, Crommelin DJ. Artificial viruses: a nanotechnological approach to gene delivery. Nat Rev Drug Discov. 2006;5(2):115–21.
13. Zuber G, Dauty E, Nothisen M, Belguise P, Behr J-P. Towards synthetic viruses. Adv Drug Del Rev. 2001;52(3):245–53.
14. Jeevanandam J, Pal K, Danquah MK. Virus-like nanoparticles as a novel delivery tool in gene therapy. Biochimie. 2019;157:38–47.
15. Rohovie MJ, Nagasawa M, Swartz JR. Virus-like particles: next-generation nanoparticles for targeted therapeutic delivery. Bioeng Transl Med. 2017;2(1):43–57.
16. Liu J, Peng Q. Protein-gold nanoparticle interactions and their possible impact on biomedical applications. Acta Biomater. 2017;55:13–27.
17. Han G, Ghosh P, Rotello VM. Functionalized gold nanoparticles for drug delivery. Nanomedicine. 2007;2(1):113–123.
18. Boisselier E, Astruc D. Gold nanoparticles in nanomedicine: preparations, imaging, diagnostics, therapies and toxicity. Chem Soc Rev. 2009;38(6):1759–82.
19. Popovtzer R, Agrawal A, Kotov NA, Popovtzer A, Balter J, Carey TE, et al. Targeted gold nanoparticles enable molecular CT imaging of cancer. Nano Lett. 2008;8(12):4593–6.
20. Grel H, Ratajczak K, Jakiela S, Stobiecka M. Gated resonance energy transfer (gRET) controlled by programmed death protein ligand 1. Nanomaterials. 2020;10(8):1592.
21. Kim HS, Lee DY. Near-infrared-responsive cancer photothermal and photodynamic therapy using gold nanoparticles. Polymers. 2018;10(9):961.
22. Bucharskaya A, Maslyakova G, Terentyuk G, Yakunin A, Avetisyan Y, Bibikova O, et al. Towards effective photothermal/photodynamic treatment using plasmonic gold nanoparticles. Int J Mol Sci. 2016;17(8):1295.
23. Yeh Y-C, Creran B, Rotello VM. Gold nanoparticles: preparation, properties, and applications in bionanotechnology. Nanoscale. 2012;4(6):1871–80.
24. Alex S, Tiwari A. Functionalized gold nanoparticles: synthesis, properties and applications—a review. J Nanosci Nanotechnol. 2015;15(3):1869–94.
25. Kopac T. Protein corona, understanding the nanoparticle–protein interactions and future perspectives: a critical review. Int J Biol Macromol. 2021;169:290–301.
26. Nghiem THL, La TH, Vu XH, Chu VH, Nguyen TH, Le QH, et al. Synthesis, capping and binding of colloidal gold nanoparticles to proteins. Adv Nat Sci Nanosci Nanotechnol. 2010;1(2):025009.
27. Gagner JE, Lopez MD, Dordick JS, Siegel RW. Effect of gold nanoparticle morphology on adsorbed protein structure and function. Biomaterials. 2011;32(29):7241–52.
28. Vonnemann J, Beziere N, Böttcher C, Riese SB, Kuehne C, Dernedde J, et al. Polyglycerolsulfate functionalized gold nanorods as optoacoustic signal nanoamplifiers for in vivo bioimaging of rheumatoid arthritis. Theranostics. 2014;4(6):629.
29. Zhang Z, Lin M. Fast loading of PEG–SH on CTAB-protected gold nanorods. RSC Adv. 2014;4(34):17760–7.
30. Mirsadeghi S, Dinarvand R, Ghahremani MH, Hormozi-Nezhad MR, Mahmoudi Z, Hajipour MJ, et al. Protein corona composition of gold nanoparticles/nanorods affects amyloid beta fibrillation process. Nanoscale. 2015;7(11):5004–13.
31. Smith DK, Korgel BA. The importance of the CTAB surfactant on the colloidal seed-mediated synthesis of gold nanorods. Langmuir. 2008;24(3):644–9.
32. Becker R, Liedberg B, Käll P-O. CTAB promoted synthesis of au nanorods–temperature effects and stability considerations. J Colloid Interface Sci. 2010;343(1):25–30.
33. Kwon K, Lee KY, Lee YW, Kim M, Heo J, Ahn SJ, et al. Controlled synthesis of icosahedral gold nanoparticles and their surface-enhanced Raman scattering property. J Phys Chem C. 2007;111(3):1161–5.
34. Khan Z, Singh T, Hussain JI, Hashmi AA. Au (III)–CTAB reduction by ascorbic acid: preparation and characterization of gold nanoparticles. Colloids Surf B Biointerfaces. 2013;104:11–7.
35. Liu K, Zheng Y, Lu X, Thai T, Lee NA, Bach U, et al. Biocompatible gold nanorods: one-step surface functionalization, highly colloidal stability, and low cytotoxicity. Langmuir. 2015;31(17):4973–80.
36. Gallina ME, Zhou Y, Johnson CJ, Harris-Birtill D, Singh M, Zhao H, et al. Aptamer-conjugated, fluorescent gold nanorods as potential cancer theradiagnostic agents. Mater Sci Eng C. 2016;59:324–32.
37. Kinnear C, Dietsch H, Clift MJ, Endes C, Rothen-Rutishauser B, Petri-Fink A. Gold nanorods: controlling their surface chemistry and complete detoxification by a two-step place exchange. Angew Chem Int Ed. 2013;52(7):1934–8.
38. Bekale L, Agudelo D, Tajmir-Riahi H. The role of polymer size and hydrophobic end-group in PEG–protein interaction. Colloids Surf B Biointerfaces. 2015;130:141–8.
39. Joshi PP, Yoon SJ, Hardin WG, Emelianov S, Sokolov KV. Conjugation of antibodies to gold nanorods through fc portion: synthesis and molecular specific imaging. Bioconjug Chem. 2013;24(6):878–88.
40. López-Gallego F, Guisán JM, Betancor L. Glutaraldehyde-mediated protein immobilization. In: Immobilization of enzymes and cells. Springer; 2013. p. 33–41.
41. Wang Y, Zhang X, Han N, Wu Y, Wei D. Oriented covalent immobilization of recombinant protein a on the glutaraldehyde activated agarose support. Int J Biol Macromol. 2018;120:100–8.
42. Sahin S, Ozmen I. Covalent immobilization of trypsin on polyvinyl alcohol-coated magnetic nanoparticles activated with glutaraldehyde. J Pharm Biomed Anal. 2020;184:113195.
43. Manson J, Kumar D, Meenan BJ, Dixon D. Polyethylene glycol functionalized gold nanoparticles: the influence of capping density on stability in various media. Gold Bull. 2011;44(2):99–105.
44. Huy TQ, Van Chung P, Thuy NT, Blanco-Andujar C, Thanh NTK. Protein A-conjugated iron oxide nanoparticles for separation of vibrio cholerae from water samples. Faraday Discuss. 2015;175:73–82.
45. Thangaraj B, Jia Z, Dai L, Liu D, Du W. Effect of silica coating on Fe3O4 magnetic nanoparticles for lipase immobilization and their application for biodiesel production. Arab J Chem. 2019;12(8):4694–706.
46. Gast M, Sobek H, Mizaikoff B. Selective virus capture via hexon imprinting. Mater Sci Eng C. 2019;99:1099–104.